Nonclassical Cosserat bending deformation of foams via holographic interferometry

R. S. Lakes
University of Wisconsin

September 12, 2023

Preprint, R. S. Lakes, Nonclassical Cosserat bending deformation of foams via holographic interferometry, Zeitschrift fur angewandte Mathematik und Physik (ZAMP), 74, 153, 3 July (2023). https://doi.org/10.1007/s00033-023-02046-1

Abstract

Nonclassical bending deformation in two foams was investigated using holographic interferometry. Sigmoid bulge deformation of the lateral surface of square cross section bars was observed. Cosserat elastic constants inferred are consistent with values obtained via size effect experiments for dense polyurethane foam. For open cell copper foam, both bulge measurements and size effects implied a large Cosserat characteristic length and a large coupling number. Limitations of the available fourth order bending analysis were encountered in this regime of strong effects.

Mathematics Subject Classification. 74A60, 74A35, 74Q15.

1 Introduction

Heterogeneous materials such as foams, composites and lattices often exhibit substantial deviations from classical elasticity. Cosserat elasticity provides sufficient freedom to represent much of the observed behavior. Classical elasticity [1] incorporates translation of points and force per area (stress). Cosserat elasticity [2] also called micropolar (with an inertia term) [3] elasticity allows more freedom than classical elasticity. Specifically, points can rotate as well as translate and there is a moment per area as well as the usual force per area. There are six elastic constants, two of which can be expressed as characteristic lengths as explained below. Cosserat elasticity is manifested in well known size effects in bending and torsion as predicted by analysis [4]. Size effects have been observed experimentally in foams [6] [7] [8] and in rib lattices [9, 10]; also in plates with a periodic array of holes [11]. One can determine from size effect measurements all six of the Cosserat elastic constants of an isotropic solid. The Cosserat characteristic length was determined in a two dimensional honeycomb [12]. The characteristic length was found to be zero in experiments on a composite containing stiff particles in a compliant matrix [4]. This result is consistent with theoretical predictions [5]. Homogenization analyses have confirmed an independent rotation variable [13] in chiral negative Poisson's ratio lattices [14].

There are also effects on the deformation field. Stress concentration factors are predicted to be reduced [15] in Cosserat solids in comparison with classical solids. Warp in torsion of square cross section bars is reduced [16] [17] in Cosserat solids. This leads to a reduction in strain concentration

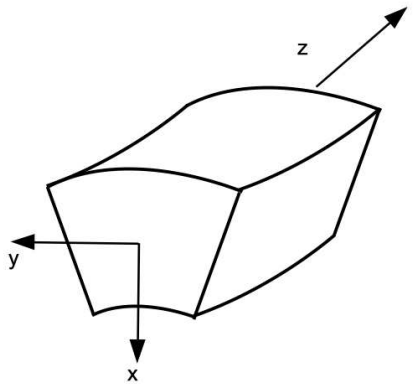

Figure 1: Classical bending deformation. Moments are applied at the flat ends in the y direction.

as has been observed in bone [18]. The warp reduction effects have been demonstrated experimentally in bone and in foams via holography [19, 20]. Asymmetry of the stress is revealed by nonzero stress and strain at the corner of the cross section. In bending of square cross section bars, the lateral surfaces bulge from Cosserat effects [21] in addition to the tilt expected [1] classically.

The constitutive equations for linear isotropic Cosserat elasticity [3] are:

$$\sigma_{ij} = 2G\epsilon_{ij} + \lambda\epsilon_{kk}\delta_{ij} + \kappa e_{ijk}(r_k - \phi_k) \tag{1}$$

$$m_{ij} = \alpha\phi_{k,k}\delta_{ij} + \beta\phi_{i,j} + \gamma\phi_{j,i} \tag{2}$$

The moment due to the asymmetric stress σ_{ij} is balanced by the couple stress, m_{ij} or moment per area. There are six independent elastic constants. G is the shear modulus in the absence of gradients; λ also has the same meaning as in classical elasticity. Sensitivity to gradients of local or micro rotation ϕ is provided by α, β, γ. The coupling between macro rotation $r_k = \frac{1}{2}e_{klm}u_{m,l}$ and micro rotation fields is quantified by κ.

Technical elastic constants, beneficial for physical insight, are: Young's modulus $E = \frac{2G(3\lambda+2G)}{2\lambda+2G}$, shear modulus G, Poisson's ratio $\nu = \frac{\lambda}{2(\lambda+G)}$, characteristic length, torsion $\ell_t = \sqrt{\frac{\beta+\gamma}{2G}}$, characteristic length, bending $\ell_b = \sqrt{\frac{\gamma}{4G}}$, coupling number $N = \sqrt{\frac{\kappa}{2G+\kappa}}$, and polar ratio $\Psi = \frac{\beta+\gamma}{\alpha+\beta+\gamma}$.

The characteristic lengths govern the length scale at which nonclassical effects become prominent. A bar of thickness 20 times the characteristic length will exhibit observable size effects [4] in torsion or bending or both. The coupling number N has a range from zero to one. It governs the magnitude of size effects and the magnitude of reductions in stress concentration. The polar ratio Ψ influences size effects in torsion.

In the present research, nonclassical bulge in bending is explored via holographic interferometry. The inferred bulge is then interpreted in terms of Cosserat elastic constants, and these are compared with constants obtained via size effect studies.

2 Analysis

The classical three-dimensional displacement field solution [1] [21] for pure bending of prismatic bars in isotropic linear elasticity is

$$u_x = -\frac{z^2 + \nu(x^2 - y^2)}{2R}, \quad u_y = -\nu\frac{xy}{R}, \quad u_z = \frac{xz}{R}, \tag{3}$$

in which R is the principal radius of curvature of bending and with ν as Poisson's ratio. Anticlastic and bend curve are in u_x. The component u_y contains the classical tilt of lateral surfaces due to Poisson's ratio. The z axis is the long axis so u_z represents longitudinal bending deformation. Figure 1 shows the bending configuration.

The nonclassical Cosserat bulge that contributes to u_y is of sigmoid shape approximated as a cubic [21]. The bulge contribution is normalized to a dimensionless quantity U as follows. The magnitude of the bulge deformation is

$$u_y^{Coss} = Ua\epsilon \tag{4}$$

with the surface strain as $\epsilon = Ma/EI$ in which E is Young's modulus in the absence of gradients, a is the bar half width; M is the applied moment and I is the area moment of inertia. It depends on the Cosserat elastic constants in a complicated way [21]. There is no sigmoid bulge of the lateral surfaces if $\beta/\gamma = -\nu$.

Size effects for $\beta/\gamma = -\nu$ with ν as Poisson's ratio are given [21] by

$$M = \frac{EI}{R}[1 + 24(\frac{\ell_b}{2a})^2(1-\nu)]. \tag{5}$$

The size effect ratio is $\Omega = MR/EI$ with E as the true Young's modulus in the absence of strain gradients. In comparison, an exact solution for bending of a round rod of a Cosserat solid [22] has the same form for $\beta/\gamma = -\nu$ but with a factor 32 rather than 24. For other β/γ the size effect equation is considerably more complicated for both round and square cross sections.

3 Methods

Two cellular solids were studied. A dense closed cell polymer foam was studied earlier in the context of size effects [6] [8]. There is a range of cell size from about 0.05 mm to about 0.15 mm in diameter. The density was 340 kg/m^3. For the present study, a square cross section specimen of the same foam was 20 mm wide and 14.2 cm long. It was clamped at one end and was oriented horizontally. Bending was achieved by dead weight load applied 41 cm from the fixed end, using a stalk attached to the free end of the specimen. The purpose was to obtain essentially pure bending in the region of observation.

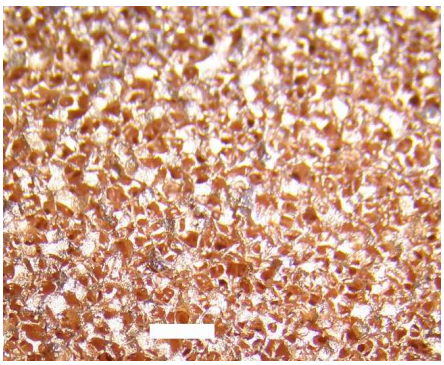

Figure 2: Copper foam. Scale bar: 2 mm.

An open cell copper foam was also studied. This was of a type previously studied [23] in the context of Poisson's ratio. The specimen was a square cross section bar 10.3 cm long by 2.4 cm by 2.4 cm wide. The mass was 24.25 g so the density is 0.41 g/cc. The corresponding relative

density (foam density divided by density of solid copper) is 0.046. Inspection of a photograph of the foam (Figure 2) indicates the cells are about 1 mm across. This specimen was cemented in vertical orientation to a massive base. Bending was achieved by dead weight load upon the end of a horizontal stalk cemented to the top of the specimen. This configuration allowed a compression test to be done as well by applying the load at the top of the specimen.

Holographic interferograms were made using photopolymer material (Litiholo) illuminated using a green laser with a wavelength of 532 nm. The laser beam was spread using a beam spreader lens of short focal length and was collimated using a large lens. The holographic plate was fixed to the center of the bar specimen via high intensity rare earth magnets. A magnet was cemented to the specimen at its center line and the plate was attached with another magnet. The purpose is to optically subtract the classical tilt deformation of the lateral surface. The center of the magnet corresponds to zero relative motion between the specimen and the holographic plate.

The experimental configuration is illustrated in Figure 3. This is the Denisyuk method which generates a reflection hologram viewable in laser light or white light. Optical components were supported on an optical table with air based vibration isolation. Two exposures were made, one of the deformed bar and one of the undeformed bar, on the same holographic plate. Holograms were then illuminated with laser light at the same wavelength as that used for exposure.

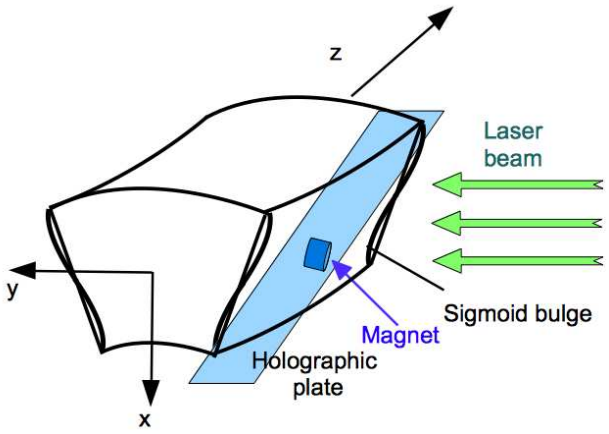

Figure 3: Bending configuration.

The static holographic fringe interpretation equation [24] is expressed in Equation 6,

$$n\lambda = \mathbf{u} \cdot (\mathbf{k}_{obs} - \mathbf{h}_{illum}) \tag{6}$$

in which $\mathbf{u}$ is the displacement vector, $\mathbf{k}_{obs}$ is the observation unit vector, λ is the wavelength, n is the fringe order and $\mathbf{h}_{illum}$ is the illumination unit vector. In the experiments, $\mathbf{h}_{illum} = \mathbf{j}$ and $\mathbf{k}_{obs}$ is chosen to reveal either u_x or u_z. In this static method, interpretation can be done using a photograph of the hologram. The nonclassical bulge in u_y contributes in either case, for all angles of view. From the theoretical plots (Figure 4), hyperbolae due to u_z are centered if the material is classical, shifted off center and skewed due to bulge if it is Cosserat. Straight fringes due to u_x become curved if there is Cosserat bulge (Figure 5).

Expressing the displacements in terms of the maximum strain ϵ, and considering the direction cosines ξ, η and ζ of the observation vector $\mathbf{k}_{obs}$,

$$n\lambda = a\epsilon[\frac{1}{2}(\frac{z}{a})^2 cos\xi + U(sin(\frac{\pi x}{a}) - \frac{\pi x}{a}))(1 + cos\eta) + \frac{x}{a}\frac{z}{a}cos\zeta] \tag{7}$$

An angle of 45 degrees was used in interpretation of the experiments for which the cosine expressions are 0.71, 1.71, 0.71.

The tilt in u_y due to the Poisson effect does not appear because the holographic plate was attached to the specimen and tilts with its surface.

The bulge is here represented as a sinusoid for which the cubic in [21] represents the first two terms. Because the holographic plate was fixed to the center of the bar specimen, it was tangent to the bar center. A linear term added to the sinusoid includes the relative displacement between plate and specimen.

The nonclassical normalized bulge U is obtained from the curvature of fringes via the deviation Δn_y from straight fringe shape evaluated at the bar surface $x = a$. The bulge obtained from fringe order contributions n_x and Δn_y is

$$U = \frac{A}{B}\frac{\Delta n_y}{n_x} \tag{8}$$

in which $A = \frac{1}{2}(\frac{z}{a})^2 cos\xi$ and $B = (sin(\frac{\pi x}{a}) - \frac{\pi x}{a}))(1 + cos\eta)$. The order n_x is the fringe count at the center of the cross section in which there is no contribution from bulge and Δn_y is determined at the edge of the cross section from the nonclassical curve of the fringes.

Similarly, the normalized bulge U is obtained from the hyperbolic fringes observed in the zy plane (angle ζ rather than ξ) by observing the shift Δn_z in the fringe pattern at the bar edge. The oblique angle of view necessitates incorporating ζ in the inference of shift.

Theoretical fringe patterns are illustrated in Figures 4 and 5.

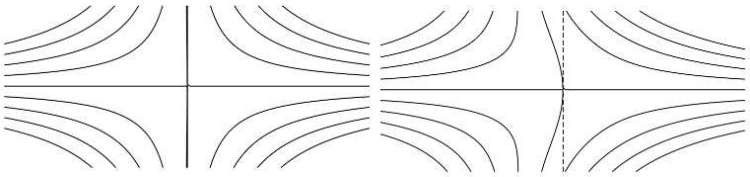

Figure 4: Theoretical fringe patterns for sensitivity in the yz plane. Left, classical; right, Cosserat. The vertical straight line through the origin represents zero displacement.

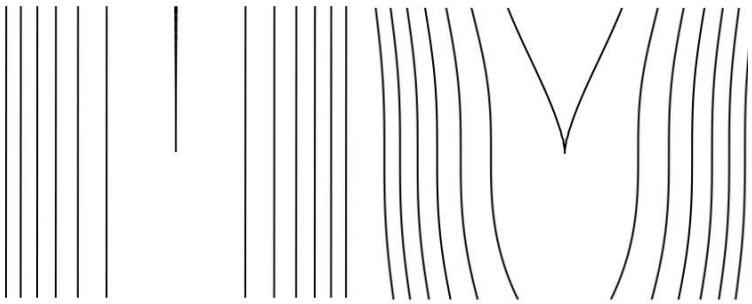

Figure 5: Theoretical fringe pattern for sensitivity in the xz plane. Left, classical; right, Cosserat.

Compression of the copper foam was done by applying a weight to the top of the specimen and was interpreted using the dynamic fringe interpretation method [24],

$$\Delta n\lambda = \mathbf{u} \cdot (\mathbf{k}_1 - \mathbf{k}_2). \tag{9}$$

The observation direction was changed from $\mathbf{k}_1$ to $\mathbf{k}_2$ and a point on the object was observed. The change Δn of the fringe order was recorded and the component of displacement $\mathbf{u}$ was inferred.

The bending modulus was determined from the static fringe pattern in the yz plane as follows. The maximum strain at the surface $x = a$ is $\epsilon = Ma/EI$ with E as the bending modulus, M as the moment and a as the bar half width. The strain is expressed as $\epsilon = \frac{u_z}{z}$ in which the increment z along the long axis is obtained from the spacing of the fringe pattern at the bar surface and u_z is obtained from Equation 6 and the known angle of observation.

4 Results

4.1 Dense polymer foam

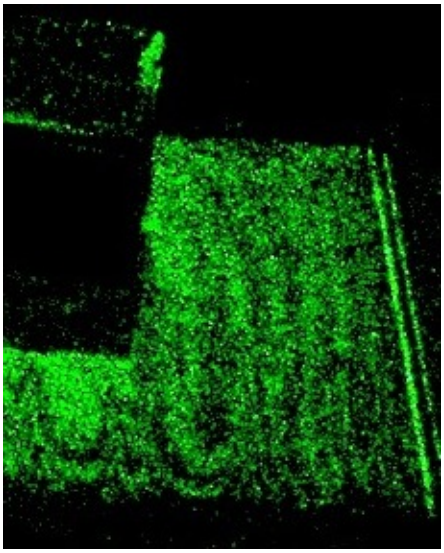

Figure 6: Experimental fringe pattern, dense polyurethane foam, sensitivity in the xz plane. The block is the magnet holding the holographic plate. Classically the fringes would be straight.

Holographic fringes for sensitivity in the xz plane are curved as shown in Figure 6, indicating a nonclassical bulge effect. Analysis of the fringe curvature for bulge contribution to u_y in dense polyurethane foam indicate the normalized bulge is $U = 0.008 \pm 0.0035$. The fourth fringe at the bar edges was used for interpretation which limited the resolution. Fringes closer to the center point of zero relative motion (the center of the magnet), though they had more curvature as anticipated had loops that were difficult to interpret. Therefore the fourth fringe was used for interpretation. Measurement of the fifth fringe yielded results similar to those from the fourth. The shift of the hyperbola pattern corresponding to u_z provided lesser resolution.

From prior size effect measurements on this kind of polymer foam [8], $\ell_b = 0.456$ mm, so ℓ_b / a $\approx 0.5/10 = 0.05$ in which a is the bar half width. With $N = 0.2$, then via [21], $U = 0.005$. In view of the resolution, this is considered a satisfactory correspondence. These size effect studies, as a result of surface layers for different shapes, admit $N = 0.15$ to 0.2. This does not obtrude in the interpretation for the following reason. For small ℓ_b in relation to the specimen width as is the case here, the predicted effect of coupling number N on the normalized bulge U is weak. For example, for $N = 0.15$, $U = 0.0042$; for $N = 0.20$, $U = 0.0048$; and for $N = 1$, $U = 0.0065$. So in this

regime of large specimen size in relation to characteristic length ℓ_b, one cannot easily discriminate among N values from bulge measurements. A smaller specimen would allow such discrimination. It is notable that even though the cell size (0.05 - 0.15 mm) is much smaller than the specimen thickness (20 mm), nonclassical effects in the bulge are observable.

4.2 Copper foam

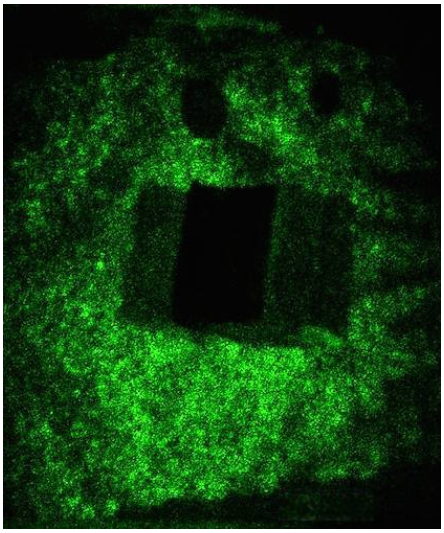

Figure 7: Experimental fringe pattern, copper foam, sensitivity in the yz plane.

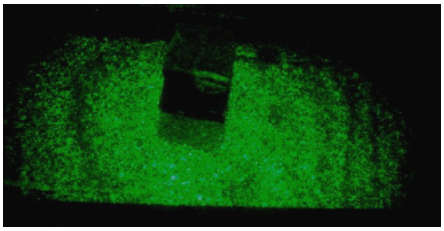

Figure 8: Experimental fringe pattern, copper foam, sensitivity in the xz plane. Classically the fringes would be straight.

Bulge of the copper foam was inferred from the observed shift of the hyperbola pattern shown in Figure 7 corresponding to u_z as follows. Recall that the point of zero relative motion is the center of the magnet used to attach the holographic plate to the specimen. The normalized bulge determined from Equation 8 referred to the xz plane is $U = 0.11 \pm 0.03$. The inferred shift incorporates a correction for shift due to the refraction of light through the 2.2 mm thick glass holographic plate via Snell's law. For the angle of view used, refraction shifts the relative position of the fringes with respect to the attached magnet. The correction was about 1/3 of the total shift.

Bulge is revealed also in the curvature of fringes observed with sensitivity in the xz plane as shown in Figure 8. From the curvature of the third fringe, $U = 0.14 \pm 0.03$ for an average with the value from the hyperbola pattern of $U = 0.125 \pm 0.03$. The fourth fringe yielded similar results.

The theory for the Cosserat bulge does not provide a unique value for each elastic constant from bulge results from a single size specimen. Prior experience with open cell foams of similar structure suggests a large value of coupling number N and a characteristic length ℓ_b larger than the cell size. For $N = 0.7$, $\nu = 0.3$, and $\beta/\gamma = 0.94$, $\frac{\ell_b}{a} = 0.4$ corresponding to $\ell_b = 5$ mm, theory predicts $U = 0.1$. Bulge theory predicts that U increases with β/γ; there is no bulge if $\beta/\gamma =$ - ν. In the present region of strong effects, increases in N above 0.7 actually reduce the predicted bulge. It is likely that effects are sufficiently strong that an exact solution rather than a fourth order solution is called for.

Size effect measurements allow inference of the characteristic length ℓ_b which contributes to the normalized bulge U. Comparison of the modulus in compression with the effective modulus in bending allows an estimate of size effects, hence ℓ_b. The inferred bending modulus was 330 MPa, and the inferred compression modulus was 93 MPa. The size effect ratio is $\Omega = 3.6$ via Equation 5 from which $\frac{\ell_b}{2a} = 0.39$ corresponding to a characteristic length $\ell_b = 9$ mm. Size effect measurements display scatter of points, so an inference from two points has considerable uncertainty but suffices to provide an order of magnitude. Also we do not have $\beta/\gamma =$ - ν for this material and attempts to use the fourth order solution were not successful. There are limitations when ℓ_b is large in that the analysis over-predicts the reduction in size effect such that the rigidity goes negative. Therefore the elementary form was used. An exact solution would be beneficial for the regime of strong effects observed here.

Detailed experimental results based on size effects are not available for this copper foam, but a polymer open cell foam [7] of cell size 0.4 mm had a bending characteristic length ℓ_b that was 5.5 times the cell size. The structure is, however, not the same as that of the copper foam.

Maximum strain levels, 5×10^{-4} for polymer foam and 10^{-4} for copper foam, were well within the linear range of behavior, so linear interpretation is justified.

Experiments with more applied load were done to obtain more fringes hence better resolution but fringe quality suffered, especially for the copper foam. Non-affine deformation is known in these foams [26]. Such deformation gives rise to grainy fringe patterns and so impairs the visibility of fringes at higher strain levels. Resolution is therefore limited.

5 Discussion

The nonclassical bulge effect in bending [21], as with the warp effect [16] [17] in torsion, is a full field effect upon the distribution of deformation. These effects are in contrast to size effects which pertain to torsion and bending rigidity. Both bulge and warp effects admit null experiments in which classical response is zero and Cosserat response is nonzero. In torsion of square cross section bars, Cosserat effects reduce the warp in comparison with the classical prediction. The classical strain at the corner of the cross section is exactly zero as a result of the symmetry of the stress. Any nonzero corner strain is nonclassical. In bending of square cross section bars, the lateral surfaces tilt as a result of Poisson effects but there is no bulge. Cosserat elasticity introduces a sigmoid shaped bulge. Any observed bulge reveals nonclassical behavior. Such nonclassical effects in warp [19, 20], strain [18] and bulge [21] have been observed.

A single measurement of sigmoid bulge in bending suffices to demonstrate nonclassical behavior and to infer a combination of ℓ_b, β/γ and N but not to infer ℓ_b and N individually. Study of specimens of several sizes is required for that.

Recall that there is no sigmoid bulge of the lateral surfaces if $\beta/\gamma = -\nu$. For normal Poisson's ratios near 1/3, that means a negative β/γ is needed for zero bulge deformation. This is permissible because the lower bound is -1. If the lower bound is approached, the torsion characteristic length

becomes small: $\ell_t << \ell_b$, a condition not found in materials studied thus far. Instead, $\beta/\gamma \to 1$ corresponding to a substantial torsion characteristic length ℓ_t and substantial bulge for Poisson's ratio near 1/3. In that vein, future studies of negative Poisson's ratio materials will be of interest.

The bulge measurement method offers high sensitivity as illustrated by the results for the dense polymer foam. The largest cells were a factor of 130 smaller than the bar width, and the smallest cells were a further factor of 3 smaller yet. Even so, nonclassical bulge effects were observed and were consistent with values anticipated via elastic constants obtained from prior size effect studies.

For open cell copper foam, bulge measurements and size effects implied a large Cosserat characteristic length and a large coupling number. Limitations of the available fourth order bending analysis were encountered in this regime of strong effects. An exact solution for the square bar would be helpful for such interpretation.

6 Conclusions

Sigmoid bulge deformation is observed in the lateral surface of square cross section bars of foams. For dense polyurethane foam, Cosserat elastic constants inferred are consistent with values obtained via prior size effect experiments. The bulge method allows observation of nonclassical effects even if the size of the microstructure is much smaller than the specimen size. Strong nonclassical effects were observed in both bulge and size effects in open cell copper foam.

The author gratefully acknowledges support of this research by the National Science Foundation via Grant No. CMMI -1906890.

References

[1] Timoshenko, S. P. and Goodier, J. N., Theory of elasticity, McGraw-Hill, New York, 3rd edition, (1970).
[2] Cosserat, E. and Cosserat, F., 1909, *Theorie des Corps Deformables*, Hermann et Fils, Paris.
[3] Eringen, A. C., Theory of micropolar elasticity. In *Fracture* 1, 621-729 (edited by H. Liebowitz), Academic Press, New York (1968).
[4] Gauthier, R. D. and W. E. Jahsman, A quest for micropolar elastic constants. J. Applied Mechanics, 42, 369-374 (1975).
[5] Bigoni, D. and Drugan, W. J.,Analytical derivation of Cosserat moduli via homogenization of heterogeneous elastic materials, J. Appl. Mech., 74, 741-753 (2007).
[6] Lakes, R. S., Experimental microelasticity of two porous solids, International Journal of Solids and Structures, 22 55-63 (1986).
[7] Rueger, Z. and Lakes, R. S., Experimental Cosserat elasticity in open cell polymer foam, Philosophical Magazine, 96 (2), 93-111, (2016).
[8] Rueger, Z. and Lakes, R. S., Experimental study of elastic constants of a dense foam with weak Cosserat coupling, Journal of Elasticity 137(1), 101-115, (2019).
[9] Rueger, Z. and Lakes, R. S., Strong Cosserat elasticity in a transversely isotropic polymer lattice, Physical Review Letters, 120, 065501 Feb. (2018).
[10] Rueger, Z., Ha C. S. and Lakes, R. S., Cosserat elastic lattices, Meccanica, 54(13), 1983-1999, (2019).
[11] Beveridge, A. J., Wheel M. A. and Nash, D. H., The Micropolar Elastic Behaviour of Model Macroscopically Heterogeneous Materials, International Journal of Solids and Structures, 50, 246-255 (2013)
[12] Mora, R. and Waas, A. M., Measurement of the Cosserat constant of circular cell polycarbonate honeycomb, Philosophical Magazine A 80,1699-1713 (2000).
[13] Spadoni, A. and Ruzzene, M., Elasto-static micropolar behavior of a chiral auxetic lattice, Journal of the Mechanics and Physics of Solids 60, 156-171 (2012).
[14] Prall, D. and Lakes, R. S., Properties of a chiral honeycomb with a Poisson's ratio -1, Int. J. of Mechanical Sciences, 39, 305-314, (1997).

[15] Mindlin, R. D., Effect of couple stresses on stress concentrations, Experimental Mech., 3, 1-7, (1963).
[16] Park, H. C., and Lakes, R. S., Torsion of a Micropolar Elastic Prism of Square Cross Section, Int. J. Solids, Struct., 23(4), 485-503, 1987.
[17] Drugan, W. J. and Lakes, R. S., Torsion of a Cosserat Elastic Bar with Square Cross-Section: Theory and Experiment, Zeitschrift fur angewandte Mathematik und Physik (ZAMP), 69(2), 24 pages (2018).
[18] Park, H. C. and Lakes, R. S., Cosserat micromechanics of human bone: strain redistribution by a hydration-sensitive constituent, J. Biomechanics, 19 385-397 (1986).
[19] Lakes, R. S., Gorman, D., and Bonfield, W., Holographic screening method for microelastic solids, J. Materials Science, 20 2882-2888 (1985).
[20] Anderson, W. B., Lakes, R. S., and Smith, M. C., Holographic evaluation of warp in the torsion of a bar of cellular solid, Cellular Polymers, 14, 1-13, (1995).
[21] Lakes, R. S. and Drugan, W. J., Bending of a Cosserat elastic bar of square cross section - theory and experiment, Journal of Applied Mechanics, 82(9), 091002 (2015). (8 pages).
[22] Krishna Reddy, G. V., and Venkatasubramanian, N. K., On the Flexural Rigidity of a Micropolar Elastic Circular Cylinder, ASME J. Appl. Mech., 45(2), 429-431, (1978).
[23] Friis, E. A., Lakes, R. S., and Park, J. B., Negative Poisson's ratio polymeric and metallic foams, Journal of Materials Science, 23, 4406-4414 (1988).
[24] Schumann W. and Dubas, M., Holographic interferometry, Springer-Verlag, Berlin, (1979).
[25] Koiter, W. T., Couple-Stresses in the theory of elasticity, Parts I and II, Proc. Koninklijke Ned. Akad. Wetenshappen 67, 17-44 (1964).
[26] Chen, C. P. and Lakes, R. S., Holographic study of non-affine deformation in copper foam with a negative Poisson's ratio -0.8, Scripta Metall et Mater., 29, 395-399, (1993).